Inorganic Chemistry

Communication

pubs.acs.org/IC

Fabrication and Catalytic Performance of Highly Stable Multifunctional Core–Shell Zeolite Composites

Xiaofang Wang,[†,‡,§] Yuanzheng Cui,[†,‡] Yang Wang,[†] Xiaowei Song,*[,†] and Jihong Yu[†]

[†]State Key Lab of Inorganic Synthesis and Preparative Chemistry, College of Chemistry, Jilin University, Changchun 130012, China

[§]Science and Technology on Surface Physics and Chemistry Laboratory, Mianyang 621907, China

Supporting Information

ABSTRACT: Multifunctional Fe_3O_4@SiO_2–Au@silicalite-1 core–shell magnetic zeolite composites were fabricated by combining a series of sol–gel process and vapor-phase transfer of silicalite-1 zeolite nanocrystal-seeded silica shells. The obtained composite has high magnetization (32.00 emu/g), stably confined and active gold nanoparticles (ca. 15 nm), and a hierarchical silicalite-1 outer shell. The core–shell composite exhibits a high efficiency of magnetic separability, excellent catalytic performance, and reusability for the reduction of 4-nitrophenol with conversion of 98% in 12 min. Moreover, it preserves a good stability after a high-temperature hydrothermal treatment.

Multifunctional composite materials with well-designed structures and diverse functions have attracted extensive research interests for their potential application in the areas of catalysis, biotechnology, nanotechnology, etc.[1] Recently, the building of core–shell structures has become a feasible technique to assemble and fabricate multifunctional composites. Taking advantage of the inherent properties of both core and shell materials, such as large surface area, electronic/optic and magnetic response, and catalytic activity, a variety of core–shell materials with integrated functions have been reported.[2]

Magnetic nanospheres (Fe_3O_4) are widely used for the preparation of core–shell materials because of their unique separable feature under an external magnetic field.[3] Recently, Yin and co-workers reported the synthesis of a Fe_3O_4@SiO_2–Au@porous SiO_2 composite with a core–shell structure, which displays both magnetism and a recyclable catalysis for the reduction of 4-nitrophenol.[4] Zhao and co-workers demonstrated another Fe_3O_4@SiO_2–Au@mesoporous SiO_2 composite, which exhibits good catalytic activity and high selectivity in liquid-phase reactions.[5] Das and Asefa synthesized a core–shell nanocatalyst consisting of a silica microsphere core decorated with gold nanoparticles (Au NPs) shell encapsulated with a porous silica shell. The resulting nanocatalyst shows an efficient heterogeneous catalysis for styrene epoxidation.[6] However, amorphous porous SiO_2 and mesoporous SiO_2 prepared by a sol–gel process have a relatively poor antihydrolysis ability and low hydrothermal stability,[7] which limited their properties and applications. Therefore, the construction of a Fe_3O_4@SiO_2–Au@shell composite with good hydrothermal stability and high antihydrolysis ability is necessary.

Silicalite-1[8] as an important member of zeolite materials with high crystallinity, excellent stability under corrosive conditions, and good thermal and hydrothermal stability is desirable for potential applications in catalysis, adsorption, separation, etc.[9] For the reasons mentioned above, it would be attractive to introduce silicalite-1 as the outer-shell material, which can integrate the collective advantages of Fe_3O_4 and Au NPs. As schematically illustrated in Scheme 1, a Fe_3O_4@SiO_2–Au@silicalite-1 multifunctional composite with a core–shell structure was fabricated by combining the sol–gel process[10] and vapor-phase transport (VPT) method.[11] This composite possesses large magnetization and stably confined active Au particles. It can be used as an efficient and recyclable catalyst to quickly catalyze 4-nitrophenol in the $NaBH_4$ aqueous solution. Moreover, it exhibits a good hydrothermal stability after a high-temperature hydrothermal treatment.

Scheme 1. Schematic Diagram Illustrating the Preparation Procedure from Fe_3O_4@SiO_2 Particles to Fe_3O_4@SiO_2–Au@silicalite-1 Particles

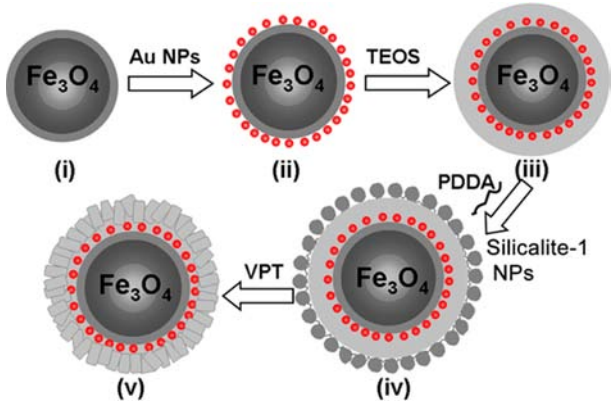

The structure and surface properties of the intermediates and Fe_3O_4@SiO_2–Au@silicalite-1 particles described in Scheme 1 were characterized by transmission electron microscopy (TEM), high-resolution TEM (HR-TEM), scanning electron microscopy (SEM), X-ray diffraction (XRD), and Fourier transform infrared (FT-IR) analyses. The TEM image of the as-synthesized Fe_3O_4 microspheres shows that the particle size of Fe_3O_4 is ca. 350 nm in diameter with a hollow interior structure (Figure 1a,b). Their

Received: May 29, 2013
Published: September 16, 2013

dx.doi.org/10.1021/ic401357s | Inorg. Chem. 2013, 52, 10708–10710

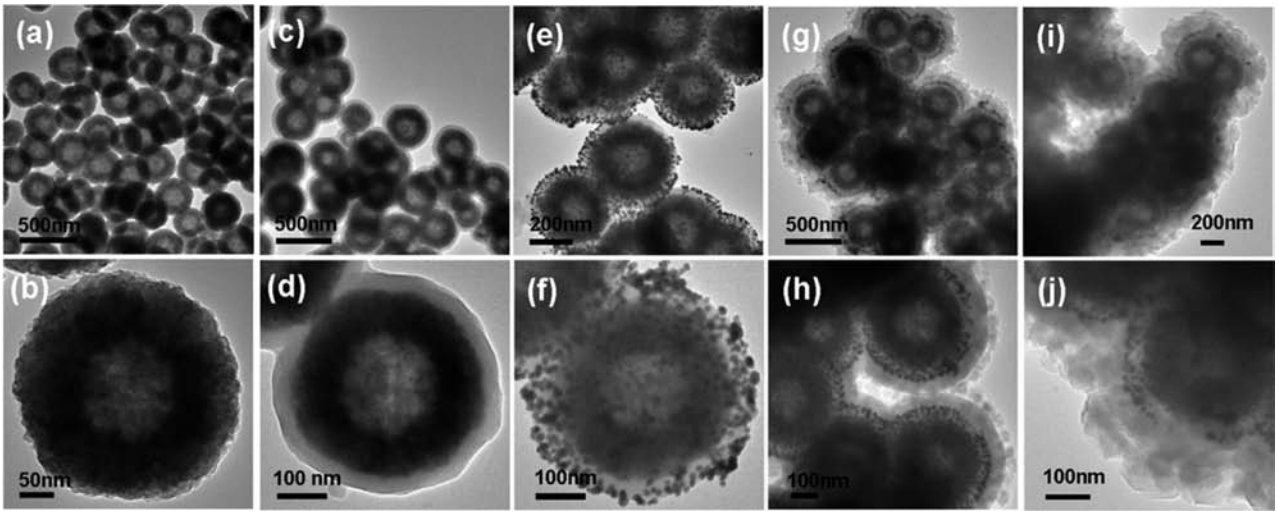

Figure 1. TEM images of (a and b) hollow Fe_3O_4, (c and d) Fe_3O_4@SiO_2, (e and f) Fe_3O_4@SiO_2−Au, (g and h) Fe_3O_4@SiO_2−Au@SiO_2-silicalite-1 NPs, and (i and j) Fe_3O_4@SiO_2−Au@silicalite-1 particles.

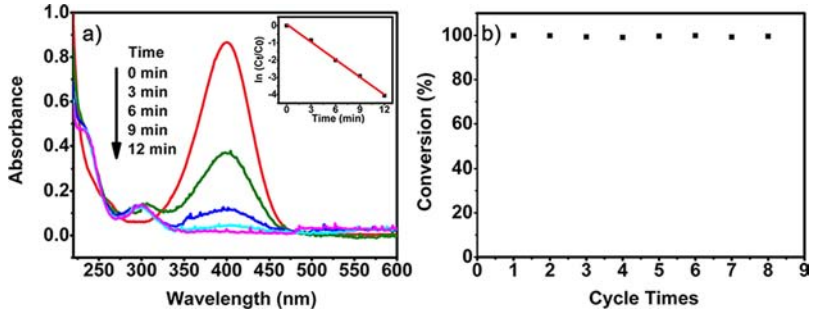

Figure 2. (a) UV/vis spectra of the reduction of 4-nitrophenol in $NaBH_4$ aqueous solution using Fe_3O_4@SiO_2−Au@silicalite-1 composites. (Inserted: Relationship between $\ln(C_t/C_0)$ and reaction time *t*. C_0 and C_t are the absorption peaks at 400 nm initially and at time *t*.) (b) Reusability of the composites for the reduction of 4-nitrophenol with $NaBH_4$.

SEM images are shown in Figure S1a in the Supporting Information (SI). The HR-TEM image shows that the magnetic microsphere is composed of a larger number of magnetic NPs as previously reported,[12] and the smaller particles are Fe_3O_4 nanocrystals with a size of ca. 8.0 nm (Figure 1b). After coating the Fe_3O_4 particles with silica shells through a modified Stöber process in ethanol,[13] core−shell particles with a smooth surface were synthesized (Figure 1c). Fe_3O_4@SiO_2 particles are uniform with a size of ca. 420 nm, and the silica layer is ca. 35 nm in thickness (Figures 1d and S1b in the SI). The surfaces of Fe_3O_4@SiO_2 particles have plentiful Si−OH groups, which could be easily modified with a monolayer of (3-aminopropyl)-triethylsilane (APTES) to chemically adsorb citrate-stabilized Au NPs because of the strong affinity between Au and amine.[14] The successful grafting of amine on Fe_3O_4@SiO_2 was confirmed by FT-IR spectra (Figure S2 in the SI). After the modification of silica with APTES, the uniform distribution of binding sites creates a homogeneous layer coating of Au NPs of ca. 15 nm, as shown in Figures 1e,f and S3 in the SI. Upon adsorption of the amphiphilic polymer poly(vinylpyrrolidone) as a coupling agent on Fe_3O_4@SiO_2−Au particles, a second layer of silica was directly coated on the particles also by a modified Stöber growth process.[15] The thickness of the exterior silica layer can be controlled by the amount of tetraethoxysilane. The outer shell of the silica coating acts as not only the template but also the starting silica source to transform into a hierarchical silicalite-1.

To transform the outer layer of silica into a crystallized silicalite-1 shell, the Fe_3O_4@SiO_2−Au@SiO_2 particles were first positively charge modified by poly(diallyldimethylammonium chloride) and then covered by silicalite-1 NPs of 40 nm diameter (Figure S4 in the SI) through electrostatic adsorption. TEM images show that the Fe_3O_4@SiO_2−Au@SiO_2 particles with silica shells of 70 nm thickness are uniformly decorated by a monolayer silicalite-1 NP (Figure 1g,h); after subsequent VPT treatment, the amorphous silica was transformed into silicalite-1 zeolites with a hierarchical structure (Figure 1i,j). SEM images of Figure S1c,d in the SI show that the size of Fe_3O_4@SiO_2−Au@silicalite-1 is of ca. 670 nm with rough surfaces because of the random growth of the silicalite-1 crystals (ca. 120 nm in thickness). The hierarchical shells of silicalite-1 zeolites are accessible for reactants to diffuse to the active sites of Au NPs. Au NPs are well-retained in the Fe_3O_4@SiO_2−Au@silicalite-1 particles, and no dramatic agglomeration of Au NPs was observed after the high-temperature VPT treatment.

As shown in Figure S5 in the SI, the XRD results show that the Fe_3O_4 NPs retain the magnetite structure (JCPDS 76-1849) during the synthetic procedures, and the characteristic diffraction peaks of face-centered-cubic Au NPs are observed. This implies that Fe_3O_4 and Au NPs are successfully fixed in the composite particles. The growth of silicalite-1 crystals on the shell is confirmed by the well-resolved peaks with higher intensities and narrower peak widths (MFI type[16]) in Figure S5e in the SI. It also indicats that the size of Au NPs is increased slightly after the high-

dx.doi.org/10.1021/ic401357s | *Inorg. Chem.* 2013, 52, 10708−10710

temperature VPT treatment by comparison of the XRD patterns of Au NPs in Figure S5d,e in the SI.

The room-temperature magnetization saturation values were measured to be 87.10 and 32.00 emu/g for hollow Fe_3O_4 particles (71.86 wt %) and Fe_3O_4@ SiO_2–Au@silicalite-1, respectively (Figure S6 in the SI). The nonlinear, reversible magnetization curves with no hysteresis at room temperature exhibit characteristic superparamagnetic behavior. Thus, the Fe_3O_4@SiO_2–Au@silicalite-1 composite can be easily manipulated by an external magnetic field, which is important for fast separation application.

We have investigated the catalytic performance of the Fe_3O_4@SiO_2–Au@silicalite-1 composite for the reduction of 4-nitrophenol in the presence of $NaBH_4$.[17] Figure 2a shows a typical UV/vis absorption change of the reaction mixture by the addition of composites. The absorption of 4-nitrophenol at 400 nm decreases with a simultaneous increase of the 300 nm peak of 4-aminophenol within 12 min. The kinetic constant k was 0.34 min^{-1} (Figure 2b), revealing that the composite has a good and high catalytic efficiency for the reduction of 4-nitrophenol. As shown in Figure 2c, the catalytic efficiency of the Fe_3O_4@SiO_2–Au@silicalite-1 composite remained nearly constant even after the eighth recycle. These results suggest that the magnetic removable Fe_3O_4@SiO_2–Au@silicalite-1 composite was not deactivated or poisoned during the catalytic or separation processes and could be recovered almost completely.

Furthermore, the hydrothermal stability of Fe_3O_4@SiO_2–Au@silicalite-1 compared to that of Fe_3O_4@SiO_2–Au@mesoporous SiO_2 prepared by the reported method[5] was studied. TEM images in Figure S7 in the SI and XRD patterns in Figure S8 in the SI show that the core–shell structure of our sample remains unchanged and the Au NPs are also well protected by the outer silicalite-1 shells after hydrothermal treatment at 140 °C for 24 h. However, the core–shell structures of the Fe_3O_4@SiO_2–Au@mesoporous SiO_2 samples are destroyed after hydrothermal treatment, as revealed by TEM images (Figure S9 in the SI). The outer mesoporous silica shells are dissolved, and dramatic agglomeration of Au NPs is observed. These results are consistent with XRD analyses (Figure S10 in the SI). As shown in Table S1 in the SI, the molar ratios of Si/Fe of our samples change slightly, but those of Fe_3O_4@SiO_2–Au@mesoporous SiO_2 are greatly reduced after hydrothermal treatment, which further confirms that the outer mesoporous silica shells of Fe_3O_4@SiO_2–Au@mesoporous SiO_2 have leached into the hot water. Moreover, the catalytic ability of Fe_3O_4@SiO_2–Au@silicalite-1 was well maintained after hydrothermal treatment (Figure S11 in the SI). Because of the highly crystalline structure of silicalite-1, the Fe_3O_4@SiO_2–Au@silicalite-1 composite has a higher hydrothermal stability, suggesting that it could be used as a good catalyst for a high-temperature hydrothermal reaction system.

In summary, we have demonstrated the fabrication of multifunctional Fe_3O_4@SiO_2–Au@silicalite-1 core–shell magnetic zeolite composites with a high magnetization, which can be easily recovered from the reaction solution using external magnetic fields. The Fe_3O_4@SiO_2–Au@silicalite-1 composite shows a good catalytic performance for the reduction of 4-nitrophenol and a high hydrothermal stability. Such composite materials with fast magnetic separation ability, high catalytic efficiency, and good hydrothermal stability, as well as excellent recyclability are expected to have promising applications in wastewater treatment, catalysis under hydrothermal conditions, and other industrial processes.

■ ASSOCIATED CONTENT

Supporting Information

Listings of experimental details, SEM and TEM images, XRD data, FT-IR spectra, magnetization hysteresis loops, UV/vis spectra, and ICP data. This material is available free of charge via the Internet at http://pubs.acs.org.

■ AUTHOR INFORMATION

Corresponding Author

*E-mail: xiaoweisong@jlu.edu.cn.

Author Contributions

‡These authors contributed equally.

Funding

This work is supported by the National Natural Science Foundation of China and the State Basic Research Project of China (Grant 2011CB808703).

Notes

The authors declare no competing financial interest.

■ REFERENCES

(1) (a) Ajayan, P. M.; Schadler, L. S.; Braun, P. V.; Picu, C.; Keblinski, P. *Nanocomposite science and technology*; Wiley-VCH Verlag GmbH & Co. KGaA: Weinheim, Germany, 2003. (b) Katz, E.; Willner, I. *Angew. Chem., Int. Ed.* **2004**, *43*, 6042–6108. (c) Čejka, J.; Mintova, S. *Catal. Rev.* **2007**, *49*, 457–509. (d) Piao, Y.; Burns, A.; Kim, J.; Wiesner, U.; Hyeon, T. *Adv. Funct. Mater.* **2008**, *18*, 3745–3758. (e) Soler-Illia, G.; Azzaroni, O. *Chem. Soc. Rev.* **2011**, *40*, 1107–1150.

(2) (a) Burns, A.; Ow, H.; Wiesner, U. *Chem. Soc. Rev.* **2006**, *35*, 1028–1042. (b) Lou, X. W.; Archer, L. A.; Yang, Z. C. *Adv. Mater.* **2008**, *20*, 3987–4019. (c) Ghosh Chaudhuri, R.; Paria, S. *Chem. Rev.* **2012**, *112*, 2373–2433.

(3) (a) Behrens, S. *Nanoscale* **2011**, *3*, 877–892. (b) Zhang, Q.; Lee, I.; Joo, J. B.; Zaera, F.; Yin, Y. *Acc. Chem. Res.* **2013**, *8*, 1816–1824.

(4) Ge, J. P.; Zhang, Q.; Zhang, T. R.; Yin, Y. D. *Angew. Chem., Int. Ed.* **2008**, *47*, 8924–8928.

(5) Deng, Y.; Cai, Y.; Sun, Z.; Liu, J.; Liu, C.; Wei, J.; Li, W.; Liu, C.; Wang, Y.; Zhao, D. *J. Am. Chem. Soc.* **2010**, *132*, 8466–8473.

(6) Das, S.; Asefa, T. *Top. Catal.* **2012**, *55*, 587–594.

(7) (a) Hench, L. L.; West, J. K. *Chem. Rev.* **1990**, *90*, 33–72. (b) Fournier, R. O.; Rowe, J. *J. Am. Mineral.* **1977**, *62*, 1052–1056. (c) Hu, Y. X.; Zhang, Q.; Goebl, J.; Zhang, T. R.; Yin, Y. D. *Phys. Chem. Chem. Phys.* **2010**, *12*, 11836–11842.

(8) Breck, D. W. *Zeolite molecular sieves: structure, chemistry and use*; Wiley: New York, 1973.

(9) (a) Davis, M. E. *Nature* **2002**, *417*, 813–821. (b) Čejka, J.; Corma, A.; Zones, S. *Zeolites and catalysis: synthesis, reactions and applications*; Wiley-VCH Verlag GmbH & Co. KGaA: Weinheim, Germany, 2010.

(10) Ciriminna, R.; Sciortino, M.; Alonzo, G.; de Schrijver, A.; Pagliaro, M. *Chem. Rev.* **2011**, *111*, 765–789.

(11) Matsukata, M.; Ogura, M.; Osaki, T.; Rao, P.; Nomura, M.; Kikuchi, E. *Top. Catal.* **1999**, *9*, 77–92.

(12) Jia, B.; Gao, L. *J. Phys. Chem. C* **2008**, *112*, 666–671.

(13) Stöber, W.; Fink, A.; Bohn, E. *J. Colloid Interface Sci.* **1968**, *26*, 62–69.

(14) (a) Liz-Marzán, L. M.; Giersig, M.; Mulvaney, P. *Langmuir* **1996**, *12*, 4329–4335. (b) Pastoriza-Santos, I.; Liz-Marzán, L. M. *Langmuir* **1999**, *15*, 948–951.

(15) Graf, C.; Dembski, S.; Hofmann, A.; Rühl, E. *Langmuir* **2006**, *22*, 5604–5610.

(16) Baerlocher, C.; McCusker, L. B.; Olson, D. *Atlas of zeolite framework types*, 6th ed.; Elsevier: Amsterdam, The Netherlands, 2007.

(17) (a) Panigrahi, S.; Basu, S.; Praharaj, S.; Pande, S.; Jana, S.; Pal, A.; Ghosh, S. K.; Pal, T. *J. Phys. Chem. C* **2007**, *111*, 4596–4605. (b) Lee, J.; Park, J. C.; Song, H. *Adv. Mater.* **2008**, *20*, 1523–1528.